Structure-Property Relationships of Oligothiophene-Isoindigo Polymers for Efficient Bulk-Heterojunction Solar Cells

Zaifei Ma, Wenjun Sun, Scott Himmelberger, Koen Vandewal, Zheng Tang, Jonas Bergqvist, Alberto Salleo, Jens Wenzel Andreasen, Olle Inganäs, Mats R Andersson, Christian Müller, Fengling Zhang and Ergang Wang

Linköping University Post Print

N.B.: When citing this work, cite the original article.

Structure–property relationships of oligothiophene–isoindigo polymers for efficient bulk-heterojunction solar cells†

Zaifei Ma,[b] Wenjun Sun,[a] Scott Himmelberger,[c] Koen Vandewal,[c] Zheng Tang,[b] Jonas Bergqvist,[b] Alberto Salleo,[c] Jens Wenzel Andreasen,[d] Olle Inganäs,[b] Mats R. Andersson,[a] Christian Müller,[a] Fengling Zhang[b] and Ergang Wang*[a]

A series of alternating oligothiophene (nT)–isoindigo (I) copolymers (PnTI) were synthesized to investigate the influence of the oligothiophene block length on the photovoltaic (PV) properties of PnTI:PCBM bulk-heterojunction blends. Our study indicates that the number of thiophene rings (n) in the repeating unit alters both polymer crystallinity and polymer–fullerene interfacial energetics, which results in a decreasing open-circuit voltage (V_{oc}) of the solar cells with increasing n. The short-circuit current density (J_{sc}) of P1TI:PCBM devices is limited by the absence of a significant driving force for electron transfer. Instead, blends based on P5TI and P6TI feature large polymer domains, which limit charge generation and thus J_{sc}. The best PV performance with a power conversion efficiency of up to 6.9% was achieved with devices based on P3TI, where a combination of a favorable morphology and an optimal interfacial energy level offset ensures efficient exciton separation and charge generation. The structure–property relationship demonstrated in this work would be a valuable guideline for the design of high performance polymers with small energy losses during the charge generation process, allowing for the fabrication of efficient solar cells that combine a minimal loss in V_{oc} with a high J_{sc}.

Broader context

Polymer solar cells (PSCs) have emerged as promising candidates for low-cost, environmentally friendly energy conversion. However, a low power conversion efficiency (PCE) is still the main bottleneck for their commercial applications. In order to further improve their PCE, a detailed understanding of the underlying structure–property relationships that govern these materials is crucial. In this work, a series of alternating oligothiophene (nT)–isoindigo (I) copolymers (PnTI) were synthesized to investigate the influence of the oligothiophene block length on the photovoltaic (PV) properties of PnTI:PCBM bulk-heterojunction blends. The driving force for the PSCs can be fine-tuned in a small range of 0–0.1 eV by changing the conjugated length of the oligothiophene block. This is a valuable guideline for polymer design to achieve high-efficiency PSCs with optimum photovoltage and photocurrent.

1. Introduction

The performance of polymer solar cells (PSCs) based on the bulk-heterojunction (BHJ)[1] concept is improving rapidly due to extensive research efforts.[2,3] When donor–acceptor (D–A) conjugated polymers, which contain alternating electron-rich and -deficient units along the polymer main chain,[4,5] are blended with fullerene derivatives, power conversion efficiencies (PCEs) of over 7–9% can be achieved.[6–8] In order to realize a high PCE, the short-circuit current density (J_{sc}), fill factor (FF) and open-circuit voltage (V_{oc}) have to be maximized at the same time. A crucial factor that determines the photovoltaic (PV) performance is the difference between the energy of the excited polymer exciton (E_{D*}) and the energy of the charge-transfer exciton (E_{CT}), or so-called driving force.[9–11] A large driving force results in a low V_{oc},[9,11,12] while an insufficient driving force can obstruct exciton dissociation and charge carrier generation, which reduces J_{sc}.[9–11] To further enhance the PV performance of PSCs, novel low band gap polymers with an optimized driving force need to be developed.[13,14] However, there is a lack of systematic studies that provide detailed synthesis guidelines for fine-tuning this driving force, especially in a small range of 0–0.1 eV.

[a]Department of Chemical and Biological Engineering/Polymer Technology, Chalmers University of Technology, SE-412 96 Göteborg, Sweden. E-mail: ergang@chalmers.se

[b]Biomolecular and Organic Electronics, IFM, Linköping University, SE-581 83 Linköping, Sweden

[c]Department of Material Science and Engineering, Stanford University, 476 Lomita Mall, Stanford, CA 94305, USA

[d]Imaging and Structural Analysis Programme, Department of Energy Conversion and Storage, Technical University of Denmark, Frederiksborgvej 399, DK-4000 Roskilde, Denmark

This journal is © The Royal Society of Chemistry 2014

Energy Environ. Sci., 2014, 7, 361–369 | 361
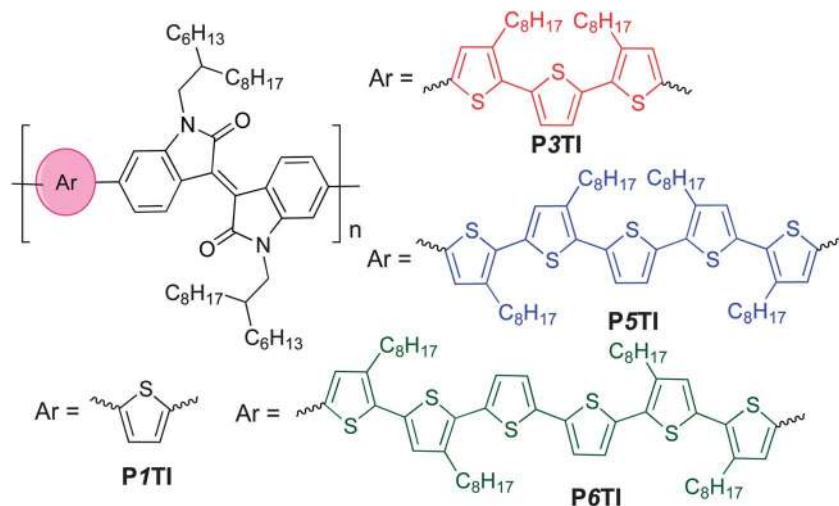
Scheme 1 The chemical structures of oligothiophene–isoindigo copolymers P*n*TI.

Isoindigo-containing D–A copolymers attract significant attention in the field of organic electronics owing to their high charge-carrier mobility.[15,16] Already widely used in the dye industry, these segments were first utilized in the photovoltaic field to build D–A small molecules in 2010,[17] followed by isoindigo-containing copolymers.[18–22] The strong electron-withdrawing nature of the isoindigo group extends the absorption spectra of copolymers to the near infrared (NIR) region.[19–22] We previously reported devices based on PTI-1 (renamed as P1TI for clarity in this work) (Scheme 1) with thiophene as the electron-rich unit and isoindigo as the electron-deficient (in the ground state) unit. PSCs based on this material had a PCE of 4.5%, with a high V_{oc} of 0.91 V but a low J_{sc} of 9.1 mA cm^{-2} due to an insufficient driving force.[9,23] Instead, when terthiophene was used as the electron-rich unit, the PCE of P3TI-based PSCs was improved to 6.3% due to a large improvement in J_{sc} to 13.1 mA cm^{-2}, which more than compensated for a decrease in V_{oc} to 0.70 V.[9,21] Evidently, despite the similar chemical structures a very different photovoltaic performance is obtained, which necessitates an in-depth investigation of relevant structure–property relationships of these oligothiophene–isoindigo polymers.

Thus, we here expand our series by synthesizing polymers with longer oligothiophene groups and carefully analyze the nanostructure and electronic properties of P*n*TI polymers as well as P*n*TI:PCBM blends using a suite of complementary characterization techniques. Our experimental results indicate that the number of thiophene rings can not only affect the energy losses during electron transfer, but also strongly influence the charge generation process due to significant variations in polymer crystallinity and active layer morphology. A sufficient driving force with minimal energy loss and optimum morphology was achieved with P3TI-based PSCs, which show a PCE of up to 6.9%.

2. Results and discussion

2.1. Synthesis and characterizations of the polymers

P*n*TI polymers were synthesized *via* the Stille coupling reaction. As depicted in Scheme 1, the number of thiophene rings ranges from 1, 3, 5 to 6. P1TI and P3TI were synthesized according to our previous reports.[20,21] Details of the synthesis of P5TI and P6TI are described in the ESI.† To ensure good solubility, octyl side chains were attached on appropriate thiophene rings. The side-chain grafting positions were chosen with the aim to avoid obvious steric hindrance. Nevertheless, attempts to synthesize P2TI and P4TI failed due to their poor solubility. The number-average molecular weights (M_n) and polydispersity index (PDI) for the P*n*TI series are listed in Table 1. All polymers are of sufficiently high molecular weight ($M_n > 60$ kg mol^{-1}) to avoid a strong influence of chain length on the PV performance.[24,25] However, we note that the $M_n \sim 100$ kg mol^{-1} of the P3TI batch used in this study is slightly higher than the $M_n \sim 43$ kg mol^{-1} of the batch in our previous report,[21] which may explain the slight improvement in PCE from 6.3 to 6.9%.

2.2. Optical properties of P*n*TI and P*n*TI:PCBM

The normalized UV-Vis absorption spectra of the four polymers in the solid state are shown in Fig. 1. Thin films of a similar thickness were spin-coated from *o*-dichlorobenzene (*o*-DCB) solutions. As shown in Fig. 1, all polymers show relatively broad absorption spectra with onsets around 800 nm and two absorption peaks in the region of 400–800 nm. The peak in the high-energy region (400–500 nm) are thought to arise from the π–π* transition on the donor segments (oligothiophene group), while the peak in the low-energy region can be attributed to an intramolecular charge transfer (ICT) transition between the donor and acceptor units.[26–28] To compare the absolute absorption coefficients of the polymers, variable-angle spectroscopic ellipsometry (VASE) was employed (see Fig. S1(b)†). All P*n*TI polymers strongly absorb in the 550–700 nm region with an absorption coefficient of $\sim 1.2 \times 10^5$ cm^{-1}. The absorption bands in the high-energy region (400–500 nm) are enhanced and red-shift with increasing *n*. This red-shift can be explained by the increase in the conjugation length of the oligothiophene block, which leads to a smaller π–π* band gap.[27,28]

362 | *Energy Environ. Sci.*, 2014, **7**, 361–369

This journal is © The Royal Society of Chemistry 2014

Table 1 Molecular weights, optical band gap and FET mobilities of PnTI

| Polymer | M_n (kg mol^{-1}) | PDI | Polymer films | As spin-coated | | Annealed at 170 °C | |
			$E_g^{opt\,a}$ (eV)	μ_h (cm^2 V^{-1} s^{-1})	μ_e (cm^2 V^{-1} s^{-1})	μ_h (cm^2 V^{-1} s^{-1})	μ_e (cm^2 V^{-1} s^{-1})
P1TI	60	2.2	1.55 ± 0.02	(8.9 ± 1.5) × 10^{-4}	(1.2 ± 0.2) × 10^{-3}	(1.0 ± 0.4) × 10^{-3}	(8.1 ± 0.6) × 10^{-3}
P3TI	100	3.3	1.50 ± 0.02	(1.8 ± 0.2) × 10^{-3}	(5.1 ± 1.1) × 10^{-4}	(3.0 ± 0.1) × 10^{-2}	(5.0 ± 1.1) × 10^{-3}
P5TI	149	3.2	1.53 ± 0.02	(8.6 ± 0.3) × 10^{-4}	(6.6 ± 2.2) × 10^{-5}	(3.6 ± 0.2) × 10^{-3}	(5.3 ± 0.2) × 10^{-4}
P6TI	67	2.6	1.52 ± 0.02	(1.7 ± 0.3) × 10^{-3}	(8.0 ± 4.0) × 10^{-5}	(7.4 ± 0.2) × 10^{-3}	(2.3 ± 1.1) × 10^{-4}

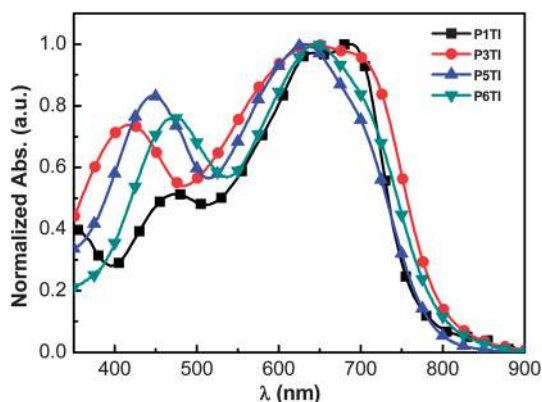^{a} The error bar is estimated from the onset of the optical band gap (~800 ± 10 nm).

Fig. 1 Normalized UV-Vis absorption spectra of PnTI films spin-coated from o-DCB solution.

The absorption coefficients of PnTI:PCBM blends were determined by VASE (Fig. 2(a)). We used PC$_{71}$BM as the acceptor for all polymers but P1TI, which was blended with PC$_{61}$BM, because this combination resulted in a better PV performance (*cf.* section "Photovoltaic performance" below).[23] The blends of P3TI, P5TI and P6TI with PC$_{71}$BM show much stronger absorption in the high-energy region (400–500 nm) compared to those with P1TI:PC$_{61}$BM, which originates from the high absorption coefficient of PC$_{71}$BM in this region. Based on the assumption that all the photons absorbed by the blends can be converted into photocurrent, one can simulate the maximum short-circuit photocurrent density ($J_{sc\text{-}max}$) that can be achieved.
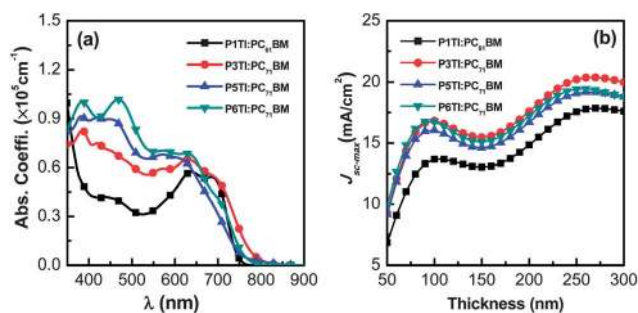
$J_{sc\text{-}max}$ calculated by the transfer matrix model (TMM)[29] is plotted in Fig. 2(b) as a function of film thickness. For all blends, two photocurrent maxima are found for a thickness of 50–300 nm. The first photocurrent maximum is located at a thickness of ~100 nm, which we consider to be the optimized thickness since charge extraction in much thicker active layers can become problematic. For P3TI, P5TI and P6TI-based blends we find a similar value of $J_{sc\text{-}max}$ ~ 16 mA cm^{-2} at the first photocurrent maximum, which indicates a comparable ability of these systems to capture photons. The lower $J_{sc\text{-}max}$ ~ 13.6 mA cm^{-2} of P1TI:PC$_{61}$BM can be explained by the weak absorption of PC$_{61}$BM in combination with a narrower absorption spectrum of P1TI (*cf.* Fig. 2(a)).

2.3. Energy levels of PnTI

Highest occupied molecular orbital (HOMO) and lowest unoccupied molecular orbital (LUMO) levels of PnTI were deduced experimentally from cyclic voltammetry (CV) on thin films from chloroform as well as theoretically from density functional theory (DFT) simulations (Fig. 3). The HOMO and LUMO positions were derived from the onset of oxidation (E^{ox}) and reduction potentials (E^{red}) obtained from CV curves according to the equations HOMO = $-(E^{ox} + 5.13)$ eV and LUMO = $-(E^{red} + 5.13)$ eV.[30] All potentials were calibrated with the standard ferrocene/ferrocenium redox couple.[31] DFT calculations were performed using Gaussian 09 with a hybrid B3LYP correlation functional[32,33] and a split valence 6-31G* basis set.[34] In order to reduce the computing time, calculations were

Fig. 2 (a) The absorption coefficient (α) spectra of PnTI:PCBM blends and (b) calculated $J_{sc\text{-}max}$ as a function of active layer thickness: P1TI:PC$_{61}$BM, P3TI:PC$_{71}$BM, P5TI:PC$_{71}$BM and P6TI:PC$_{71}$BM.
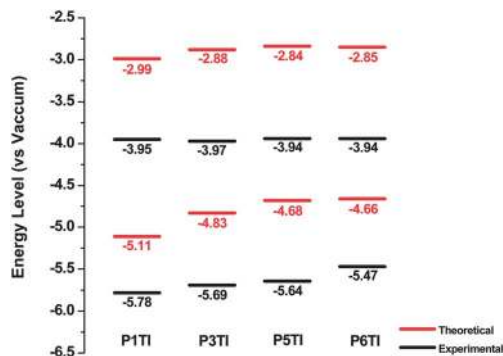

Fig. 3 Theoretical and experimental energy levels of PnTI from cyclic voltammetry measurements and DFT calculations.

This journal is © The Royal Society of Chemistry 2014

Energy Environ. Sci., 2014, **7**, 361–369 | **363**

performed for trimers containing three repeating units with methyl groups instead of long octyl side chains.

Our DFT calculations show that the trimer, which corresponds to P1TI, has a slightly lower LUMO level compared to the other three trimers. However, the LUMO levels as measured by CV are nearly identical. This is consistent with a previous report by Blouin et al., which demonstrates that LUMO levels are mainly determined by electron-deficient units but are only slightly influenced by electron-rich units.[35] On the other hand, differences can be found in the HOMO levels as revealed by both CV measurements and DFT calculations, which is likely to affect the V_{oc} of PnTI-based PSCs.[36] Moreover, our DFT calculations suggest that all modeled trimers have largely planar backbones, favorable for π-stacking, as depicted by the side view of the optimal molecular conformations at 0 K in the gas phase (Fig. S3†).

2.4. Photovoltaic performance

The PSCs studied in this work are prepared in the conventional device geometry (ITO/PEDOT:PSS/active layer/LiF/Al). The PV performance of each PnTI:PCBM active layer was optimized by choosing different acceptors (PC$_{61}$BM/PC$_{71}$BM), processing solvents, and D–A stoichiometry. The optimized D : A weight ratio for all the polymers is 2 : 3 and the processing solvents are o-DCB containing 2.5% (by volume) diiodooctane (DIO). DIO was added because according to a number of previous reports the morphology of the active layer can be improved.[37,38] In this work we compare the results obtained from fully optimized PSCs. Therefore, PC$_{61}$BM is used for P1TI-based PSCs and PC$_{71}$BM for devices based on the other three PnTI polymers.[20,21,23] According to the optical simulation results shown in Fig. 2(b), the optimal active layer thickness is around 100 nm for all PnTI:PCBM blends.

The current density–voltage (J–V) curves from optimized PSCs are plotted in Fig. 4 and the corresponding PV parameters are listed in Table 2. Statistical deviations of the PV parameters for PnTI:PCBM solar cells are given in Fig. S4.† The device with P1TI:PC$_{61}$BM as the active layer has the lowest PCE of 4.3%, whereas the P3TI:PC$_{71}$BM device exhibits the highest PCE of 6.9%. The slightly higher efficiency compared to our previous report (6.3%) can be ascribed to the higher molecular weight of
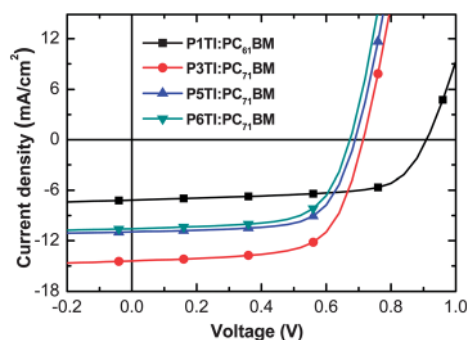

Fig. 4 J–V curves of devices based on P1TI:PC$_{61}$BM, P3TI:PC$_{71}$BM, P5TI:PC$_{71}$BM and P6TI:PC$_{71}$BM.

P3TI used in this work.[39,40] Lower PCEs are obtained for PSCs with P5TI:PC$_{71}$BM and P6TI:PC$_{71}$BM. The V_{oc} of the devices decreases from 0.91 to 0.65 V when n increases from 1 to 6, which is consistent with the observed trend in HOMO levels (cf. Fig. 3). We obtain the highest J_{sc} for a champion PSC based on P3TI:PC$_{71}$BM, which outperforms the devices based on PnTI with both a shorter and a longer oligothiophene block. The $J_{sc} \sim$ 14.63 mA cm^{-2} of this device is close to the modeled $J_{sc\text{-}max} \sim$ 16.8 mA cm^{-2}. In contrast, optimum PSCs based on the other three polymers display a larger difference between J_{sc} and modeled $J_{sc\text{-}max}$. We can identify three possible reasons for the apparent loss in generated current-density: (i) the polymer charge-carrier mobility is too low, (ii) the driving force for charge separation is insufficient, and (iii) the morphology of the active layers is non-optimal. In the following, we investigate these three arguments in detail with the aim to identify the origin for the observed PV performance.

2.5. Mobilities of PnTI from field effect transistor (FET) measurements

Optimized PSCs based on PnTI:PCBM feature similar and high FFs ~ 0.66, which suggests that the difference in J_{sc} of these devices is not limited by insufficient charge carrier mobilities (similar active layer thicknesses of about 100 nm are used for all the devices).[41,42] To gain further insight, we measured the hole and electron mobilities of PnTI polymers in bottom-gate, bottom-contact field-effect transistors (FETs). Active layers were spin-coated from chloroform and annealed for one hour at 170 °C according to Mei et al., who found that this treatment optimizes the FET mobilities of thiophene-isoindigo copolymers.[16] As summarized in Table 1, all polymers displayed a comparable hole mobility $\mu_h \sim 10^{-3}$ cm^2 V^{-1} s^{-1} after spin-coating from chloroform. The hole mobility of all four polymers increased after annealing at 170 °C, which is likely due to improved molecular packing (cf. discussion on crystalline order below). The highest $\mu_h \sim 3 \times 10^{-2}$ cm^2 V^{-1} s^{-1} was obtained for P3TI, although its high mobility does not seem to be the primary factor behind the high J_{sc} of optimized PSCs based on the same polymer. Interestingly, all PnTI polymers display ambipolar behavior. The electron mobility μ_e decreases with the number of thiophene rings from $\mu_e \sim 8 \times 10^{-3}$ cm^2 V^{-1} s^{-1} for P1TI to $\mu_e \sim 2 \times 10^{-4}$ cm^2 V^{-1} s^{-1} for P6TI.[43] As shown in Fig. S3,† HOMO and LUMO orbitals of P1TI can delocalize over the whole backbone of the modeled trimer, which indicates that efficient intrachain transport of electrons as well as holes is feasible. The larger overlap of the HOMO and LUMO orbitals of P1TI can also explain its higher absorption coefficient (Fig. S3 and S1(b)†).[43,44]

2.6. Energy of charge transfer state and device V_{oc}

The energy of the charge transfer (CT) state (E_{CT}) is considered to be the effective band gap of a D–A blend and determines the V_{oc} of a BHJ organic solar cell.[11,45–48] Generally, E_{CT} depends on the difference between the LUMO level of the acceptor and the HOMO level of the donor, with significant contributions from D–A material interactions. It can be deduced from

Table 2 PV parameters, active layer thickness, EQE_{EL} and driving force of optimized PSCs based on PnTI:PCBM blends

Active layer	J_{sc} (mA cm^{-2})	FF	V_{oc} (V)	PCE (%)	EQE_{EL}	V_{oc}^{rad} (eV)	E_{CT} (eV)	E_{D*}^{a} (eV)	Driving force^{b} (eV)
P1TI:PC$_{61}$BM	7.16	0.66	0.91	4.30	7.0×10^{-7}	1.27	1.55	1.55 ± 0.02	0.00 ± 0.02
P3TI:PC$_{71}$BM	14.63	0.66	0.72	6.90	1.5×10^{-8}	1.17	1.45	1.50 ± 0.02	0.05 ± 0.02
P5TI:PC$_{71}$BM	11.28	0.67	0.69	5.26	6.0×10^{-9}	1.15	1.43	1.53 ± 0.02	0.10 ± 0.02
P6TI:PC$_{71}$BM	10.51	0.66	0.65	4.65	4.0×10^{-9}	1.12	1.40	1.52 ± 0.02	0.12 ± 0.02

^{a} The error bar for E_{D*} is from the energy of the optical band gap of PnTI ($E_{D*} = E_g^{opt}$). ^{b} The error bar for the driving force is from E_{D*} (driving force = $E_{D*} - E_{CT}$).

electroluminescence (EL) measurements[49] or from the external quantum efficiency (EQE) measured in the low energy sub-optical gap region with highly sensitive techniques, such as Fourier-transform photocurrent spectroscopy (FTPS).[50] However, when E_{CT} of the BHJ blend is very close to the energy of the polymer exciton (E_{D*}), such as for the PnTI:PCBM systems, it becomes more difficult to distinguish CT absorption and emission bands from the local donor excitations. As shown in Fig. S5,† a broadening of the absorption tail but no distinct CT absorption bands can be detected using FTPS-EQE spectra, indicating that the CT absorption is masked by the absorption of the neat PnTI material. However, the red-shifted EL of the blends as compared to that of the pure polymers indicates that low energy CT states are present.

Since the CT band and local donor excitations overlap, we estimate E_{CT} via the V_{oc} obtained for the blend by using eqn (1) and (2).[51–53] V_{oc}^{rad} is the open-circuit voltage when radiative recombination is the sole loss mechanism.

$$V_{oc}^{rad} = V_{oc} - \frac{kT}{q}\ln(EQE_{EL}) \tag{1}$$

V_{oc}^{rad} for all PnTI:PCBM-based PSCs is obtained, which permitted us to deduce E_{CT} from eqn (2):

$$V_{oc}^{rad} = \frac{E_{CT}}{q} + \frac{kT}{q}\ln\left(\frac{J_{sc}h^3c^2}{fq2\pi(E_{CT} - \Phi)}\right) \tag{2}$$

here, k is the Boltzmann's constant, q is the elementary charge, T is the absolute temperature, EQE_{EL} is the radiative recombination efficiency, which is measured as the external quantum efficiency of electroluminescence as listed in Table 2, h is the Planck constant, f is a prefactor, which is proportional to the electronic coupling matrix element squared and the interfacial area, and Φ is the reorganization energy. Provided that the electronic coupling of donor–acceptor f is within the same order of magnitude for all PnTI:PCBM blends, the loss of V_{oc} due to recombination depends weakly on E_{CT}. As a result, the second term in eqn (2) can be regarded as a constant and we obtain eqn (3):

$$V_{oc}^{rad} = \frac{E_{CT}}{q} + \text{const.} \tag{3}$$

Thus, E_{CT} of the PnTI:PCBM blends can be estimated from V_{oc}^{rad} (Table 2). The constant can be deduced from the fact that the E_{CT} of the P1TI:PCBM system is equal to E_{D*} since the driving force ($E_{D*} - E_{CT}$) is close to ~0.0 eV, as indicated by the

absence of any redshift in the blend EL spectrum as compared to pure P1TI.[9] As summarized in Table 2, E_{CT} of the PnTI:PCBM blends decreases with the number of thiophene rings in the repeating unit, while losses due to a non-radiative recombination increase with the number of thiophene rings. Both effects contribute to the reduction in V_{oc} with increasing n.

2.7. Driving force and exciton dissociation

Once E_{CT} is known, the driving force for exciton dissociation can be estimated by the difference between E_{D*} and E_{CT} ($E_{D*} - E_{CT}$).[9,11] Here, E_{D*} is equal to the optical band gap of the polymers. For the solar cell based on P3TI:PC$_{71}$BM an internal quantum efficiency (IQE) of ~90% can be obtained despite a low driving force of only ~0.1 eV. In the present work, we find that the driving force $E_{D*} - E_{CT}$ of PnTI:PCBM based PSCs increases with the number of thiophene rings in the repeating unit as listed in Table 2. The data are consistent with the comparison of EL spectra of the PSCs fabricated from pure PnTI polymers and PnTI:PCBM blends. The EL of blend-based devices is red-shifted due to the presence of CT emission bands, whereas the EL of the devices based on pure PnTI arises from polymer exciton emission only (Fig. S6†).[49] Thus, the offset between emission peaks of the pure polymer and the corresponding blend is proportional to the driving force. As shown in Fig. S6,† this offset increases with n.

However, despite the increased driving force of P5TI:PC$_{71}$BM and P6TI:PC$_{71}$BM blends the overall exciton dissociation is insufficient, as indicated by the photoluminescence (PL) measurements (Fig. S7†). PL quenching efficiencies (ΔPL) were calculated according to eqn (4):

$$\Delta PL = 1 - \frac{PL_{blend}}{PL_{PnTI}} \tag{4}$$

where PL_{blend} and PL_{PnTI} are the integrated relative PL counts of PnTI:PCBM blends and pure PnTI, respectively. We estimate the largest ΔPL ~ 90% for the P3TI system, which is in strong contrast to a significantly lower value of ~70%, ~80% and ~65% for the P1TI, P5TI and P6TI system, respectively. This observation suggests that exciton dissociation is the most efficient in P3TI:PC$_{71}$BM blends, which is consistent with the high J_{sc}. To investigate whether the low PL quenching efficiency of the remaining blends is due to insufficient exciton diffusion or interfacial exciton dissociation, we measured field-dependent PL quenching under the application of a negative bias voltage.[54] The relative integrated PL counts as a function of

This journal is © The Royal Society of Chemistry 2014

Energy Environ. Sci., 2014, **7**, 361–369 | **365**

applied negative voltage are plotted in Fig. 5. As expected, the PL quenching behavior of all pure polymer devices does not vary with the applied field. For the examined P1TI:PC$_{61}$BM device we observe that a substantial amount of PL emission is quenched when high negative voltages are applied. We conclude that the low driving force prevents excitons that have reached the P1TI:PC$_{61}$BM interface from eventually dissociating into free charge carriers. For such a low driving force, back electron transfer of the system from CT state to D* state is likely and competes with CT state dissociation into free carriers. Such a singlet exciton regeneration has been observed previously.[55] However, once an external driving force is provided by a high electric field, the dissociation of CT states is facilitated and D* regeneration and subsequent emission are prevented. This results in a much higher quenching efficiency ΔPL of ∼ 85% for a bias voltage of −8 V. In significant contrast, P3TI:PC$_{71}$BM, P5TI:PC$_{71}$BM and P6TI:PC$_{71}$BM based devices display a constant quenching efficiency with increasing reverse voltage, which indicates that the observed inefficient exciton dissociation is not caused by a lack of driving force. We therefore ascribe the reason for the low quenching efficiency to the existence of large polymer domains in the blends, which prevent excitons from reaching the D–A interface before exciton recombination occurs. In the next section we use a combination of IQE, transmission electron microscopy (TEM) and grazing-incidence wide-angle X-ray scattering (GIWAXS) measurements to verify this argument.

2.8. Quantum efficiency and morphology

IQE is a suitable tool to separate absorption losses from charge generation and recombination losses under short-circuit conditions. IQE calculations were conducted based on EQE measurements, using eqn (5):

$$IQE(\lambda) = \frac{EQE(\lambda)}{1 - A_{para}(\lambda) - R(\lambda)} \qquad (5)$$

where $EQE(\lambda)$ and $R(\lambda)$ are the measured EQE and reflectance of the PSCs, respectively, and $A_{para}(\lambda)$ is the parasitic electrode absorption deduced from TMM.[29,56] We find that the highest IQE for PSCs is based on P3TI:PC$_{71}$BM, while P1TI:PC$_{61}$BM devices display the lowest IQE (Fig. 6), since exciton dissociation

is limited due to the low driving force. It is worth noting that the IQE of PSCs based on P5TI:PC$_{71}$BM and P6TI:PC$_{71}$BM is not only lower than that of the P3TI:PC$_{71}$BM devices, but also wavelength dependent. Burkhard *et al.* have reported that the IQE of P3HT:PC$_{61}$BM based PSCs is lower at wavelengths, at which PC$_{61}$BM absorbs. This was rationalized by the existence of large PC$_{61}$BM domains in combination with a short exciton diffusion length in PC$_{61}$BM.[57] Instead, for the here investigated blends we observe that the IQE is higher at wavelengths, at which PC$_{71}$BM strongly absorbs. This observation is consistent with the presence of large polymer domains in P5TI:PC$_{71}$BM and P6TI:PC$_{71}$BM blends and implies the absence of large PC$_{71}$BM domains. This argument is consistent with the absence of PL from PCBM (Fig. S7†), which indicates that all PCBM excitons are converted to D* excitons or dissociate into free charge carriers. Furthermore, TEM images suggest that the nanostructure coarsens with increasing length of the oligo-thiophene block (Fig. 7), which is consistent with our PL quenching experiments.

To investigate the reason for the existence of large polymer domains in PnTI:PCBM blends, we studied the thermal behavior of PnTI polymers with differential scanning calorimetry (DSC). Recorded heating thermograms display a clear melting endotherm at elevated temperature, which suggests that all four polymers are semi-crystalline (Fig. S8† and Table 3). The peak melting temperature decreases from $T_m \sim 321\ ^\circ$C for P1TI to $T_m \sim 289\ ^\circ$C for P3TI and $T_m \sim 226\ ^\circ$C for P5TI, which we ascribe to the increasing number of alkyl-substituted thiophene
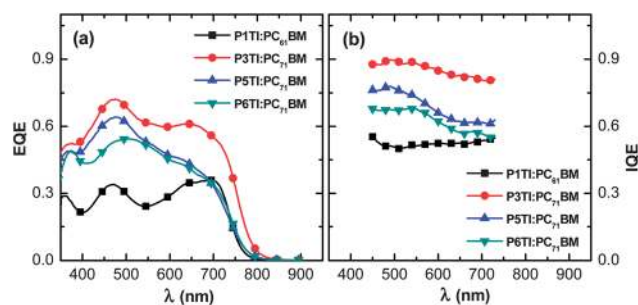

Fig. 6 (a) EQE and (b) IQE spectra for P1TI:PC$_{61}$BM, P3TI:PC$_{71}$BM, P5TI:PC$_{71}$BM and P6TI:PC$_{71}$BM based PSCs.
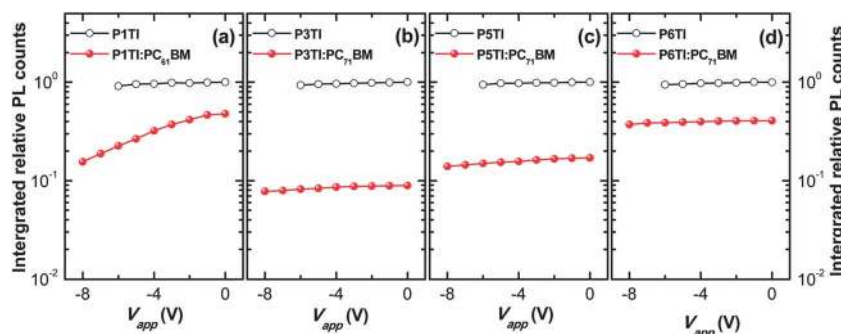

Fig. 5 Integrated relative PL counts obtained from devices based on pure PnTI (open circles) and PnTI:PCBM blends (solid circles) under a reverse bias voltage for (a) P1TI, (b) P3TI, (c) P5TI and (d) P6TI system.
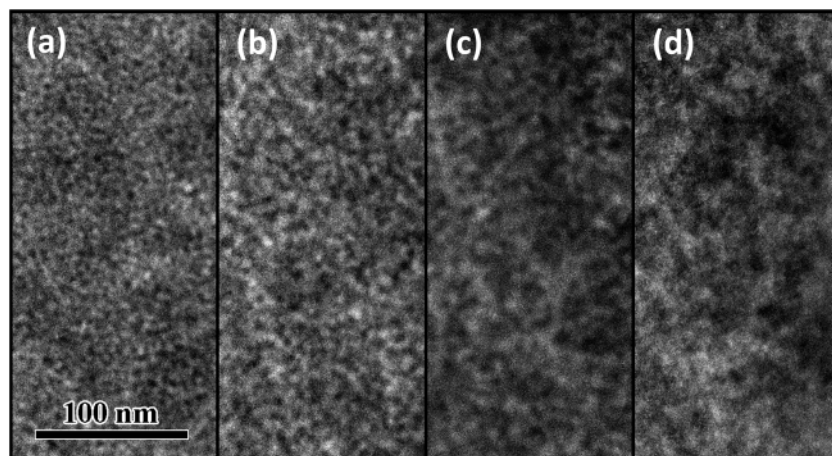
366 | *Energy Environ. Sci.*, 2014, **7**, 361–369

This journal is © The Royal Society of Chemistry 2014

Fig. 7 TEM images of (a) P1TI:PC$_{61}$BM, (b) P3TI:PC$_{71}$BM, (c) P5TI:PC$_{71}$BM and (d) P6TI:PC$_{71}$BM. All active layers are prepared from o-DCB:DIO (2.5% by volume) solutions.

rings. In contrast, the addition of a second unsubstituted thiophene ring to the backbone again raises the melting temperature of P6TI to $T_m \sim 272\ ^{\circ}\text{C}$. Moreover, we note that the observed melting transitions of P1TI and P3TI feature the highest enthalpy of fusion $\Delta H_f \sim 24\ \text{J g}^{-1}$, which highlights the ability of these polymers to order.

In a further set of experiments we carried out GIWAXS of pure PnTI as well as optimized PnTI:PCBM blend films (Fig. S9†). GIWAXS patterns of all four polymers reveal distinct diffractions at $q_{100} \sim 0.3\ \text{Å}^{-1}$ and $q_{010} \sim 1.7\ \text{Å}^{-1}$, which we interpret as lamellar and π-stacking with $d_{100} \sim 20\ \text{Å}$ and $d_{010} \sim 3.7\ \text{Å}$, respectively (Table 3; we assume an orthorhombic unit cell and use $d = 2\pi/q$). Moreover, we observe a slight preference for a face-on texture, which increases with the number of thiophene rings. We used the Scherrer equation[58] to estimate the coherence length (D) of prominent scattering signals. The coherence length of π-stacking is similar for all PnTI polymers and for P3TI we estimate the largest $D_{010} \sim 29\ \text{Å}$, which implies that the polymer is able to maintain crystalline coherence in the π-stacking direction for at least 9 backbone segments. Interestingly, for the widely studied semi-crystalline donor polymer P3HT, a comparable π-stacking coherence length on the order of ~ 4 nm has been reported.[59] Closer analysis of the lamellar stacking signal reveals a similar trend with $D_{100} \sim 209\ \text{Å}$ for P3TI, which corresponds to a coherent ordering of 11 lamellar stacks.

GIWAXS patterns of optimized PnTI:PCBM blend films reveal a predominantly isotropic texture (Fig. S9† and Table 4). The [100] signal of the polymer can be clearly discerned and we were

Table 4 Structural parameters of optimum PnTI:PCBM blends

	PCBM		PnTI		
	q_{PCBM} (Å^{-1})	D_{PCBM} (Å)	d_{100} (Å)	D_{100} (Å)	100 texture (—)
P1TI:PC$_{61}$BM	1.39	30	19	63	Isotropic
P3TI:PC$_{71}$BM	1.35	30	20	48	Isotropic
P5TI:PC$_{71}$BM	1.35	30	20	90	Isotropic
P6TI:PC$_{71}$BM	1.35	33	18	105	Edge-on

able to calculate the coherence length of lamellar stacking. P3TI:PC$_{71}$BM features the smallest $D_{100} \sim 48\ \text{Å}$. In contrast, for P5TI:PC$_{71}$BM and P6TI:PC$_{71}$BM blends we find a significantly larger coherence length, which implies the existence of larger polymer crystallites. This observation is consistent with the much reduced PL quenching that we have recorded. Furthermore, the GIWAXS patterns of all blends feature two prominent halos around $q \sim 0.8\ \text{Å}^{-1}$ and $q \sim 1.4\ \text{Å}^{-1}$ that are characteristic of amorphous PCBM[60] and therefore suggest the presence of phase-separated, PCBM-rich domains. The amorphous character of PCBM is consistent with the short coherence length of $D_{PCBM} \sim 30\ \text{Å}$ found in all samples (note that the outer diameter of the C$_{60}$ cage is about 10 Å),[61] which indicates that no significant difference in PCBM packing exists between blends.

A combination of PL, DSC, GIWAXS and TEM measurements verified that the lower IQE of devices based on P5TI:PC$_{71}$BM and P6TI:PC$_{71}$BM at long wavelength results from the coarse active layer morphology, particularly, the large polymer domains in their blends, which prevents excitons generated in the polymer phase from reaching the D–A interface.

3.   Conclusions

A series of D–A polymers based on oligothiophene and iso-indigo units were synthesized and PSCs with efficiencies approaching 7% were fabricated, which indicates that this class

Table 3 Structural parameters of PnTI spin-coated from chloroform and annealed for one hour at 170 $^{\circ}$C

	T_m ($^{\circ}$C)	T_c ($^{\circ}$C)	ΔH_f (J g^{-1})	d_{100} (Å)	D_{100} (Å)	d_{010} (Å)	D_{010} (Å)	010 texture ($^{\circ}$)
P1TI	321	—	24	20	67	3.7	22	43
P3TI	289	220	24	21	209	3.7	29	33
P5TI	226	177	12	21	180	3.8	22	34
P6TI	272	227	19	19	175	3.7	25	29

This journal is © The Royal Society of Chemistry 2014

Energy Environ. Sci., 2014, **7**, 361–369 | **367**

of polymers are promising materials for PV applications. The relationship between the polymer structure and the PV performance was investigated *via* a comprehensive study using a number of complementary methods, such as optical modeling and IQE calculations by TMM, luminescence measurements, TEM and GIWAXS. Although the four polymers have similar chemical structures, optimized PSCs display significant differences in V_{oc} and J_{sc}. The P1TI:PC$_{61}$BM based device exhibits a relatively high V_{oc}, but low J_{sc} and IQE, due to an insufficient driving force for exciton dissociation. PSCs based on P5TI:PC$_{71}$BM and P6TI:PC$_{71}$BM have a lower V_{oc} due to the larger energy loss in the exciton dissociation mechanism (driving force). This is consistent with their higher HOMO levels, which means that the increase in conjugation length of the oligothiophene donor segments can be used to raise the HOMO level of the polymers. However, low J_{sc}s are obtained for these PSCs. It was found that large polymer domains in the active layers limit the number of excitons that can diffuse to the D–A interface. A solar cell based on P3TI:PC$_{71}$BM displayed the highest efficiency due to the appropriate driving force and optimal morphology of this system in combination with adequately sized polymer domains. This work confirms that the driving force for efficient charge separation can be as low as ~0.1 eV, which can be tuned by molecular design, *i.e.* by changing the length of the oligothiophene donor segment. This provides a valuable pathway to minimize the energy loss required for exciton separation (driving force) to ensure a high J_{sc} without any unnecessary loss in V_{oc}. The relationship between polymer structures and their PV properties revealed in this work is a valuable guideline for polymer design aimed at achieving high-efficiency PSCs with optimum V_{oc} and J_{sc}.

Acknowledgements

References

1 G. Yu, J. Gao, J. C. Hummelen, F. Wudl and A. J. Heeger, *Science*, 1995, **270**, 1789–1791.

2 G. Li, R. Zhu and Y. Yang, *Nat. Photonics*, 2012, **6**, 153–161.

3 Y. Li, *Acc. Chem. Res.*, 2012, **45**, 723–733.

4 K. Colladet, S. Fourier, T. J. Cleij, L. Lutsen, J. Gelan, D. Vanderzande, L. Huong Nguyen, H. Neugebauer, S. Sariciftci, A. Aguirre, G. Janssen and E. Goovaerts, *Macromolecules*, 2007, **40**, 65–72.

5 Z.-G. Zhang and J. Wang, *J. Mater. Chem.*, 2012, **22**, 4178–4187.

6 Z. He, C. Zhong, S. Su, M. Xu, H. Wu and Y. Cao, *Nat. Photonics*, 2012, **6**, 591–595.

7 C. Cabanetos, A. El Labban, J. A. Bartelt, J. D. Douglas, W. R. Mateker, J. M. J. Fréchet, M. D. McGehee and P. M. Beaujuge, *J. Am. Chem. Soc.*, 2013, **135**, 4656–4659.

8 M. A. Green, K. Emery, Y. Hishikawa, W. Warta and E. D. Dunlop, *Prog. Photovoltaics*, 2013, **21**, 1–11.

9 K. Vandewal, Z. Ma, J. Bergqvist, Z. Tang, E. Wang, P. Henriksson, K. Tvingstedt, M. R. Andersson, F. Zhang and O. Inganäs, *Adv. Funct. Mater.*, 2012, **22**, 3480–3490.

10 M. A. Faist, T. Kirchartz, W. Gong, R. S. Ashraf, I. McCulloch, J. C. de Mello, N. J. Ekins-Daukes, D. D. C. Bradley and J. Nelson, *J. Am. Chem. Soc.*, 2012, **134**, 685–692.

11 D. Veldman, S. C. J. Meskers and R. A. J. Janssen, *Adv. Funct. Mater.*, 2009, **19**, 1939–1948.

12 W. Li, W. S. C. Roelofs, M. M. Wienk and R. A. J. Janssen, *J. Am. Chem. Soc.*, 2012, **134**, 13787–13795.

13 F. He and L. Yu, *J. Phys. Chem. Lett.*, 2011, **2**, 3102–3113.

14 P. Kumar and S. Chand, *Prog. Photovoltaics*, 2012, **20**, 377–415.

15 T. Lei, Y. Cao, X. Zhou, Y. Peng, J. Bian and J. Pei, *Chem. Mater.*, 2012, **24**, 1762–1770.

16 J. Mei, D. H. Kim, A. L. Ayzner, M. F. Toney and Z. Bao, *J. Am. Chem. Soc.*, 2011, **133**, 20130–20133.

17 J. Mei, K. R. Graham, R. Stalder and J. R. Reynolds, *Org. Lett.*, 2010, **12**, 660–663.

18 R. Stalder, J. Mei, J. Subbiah, C. Grand, L. A. Estrada, F. So and J. R. Reynolds, *Macromolecules*, 2011, **44**, 6303–6310.

19 G. Zhang, Y. Fu, Z. Xie and Q. Zhang, *Macromolecules*, 2011, **44**, 1414–1420.

20 E. Wang, Z. Ma, Z. Zhang, P. Henriksson, O. Inganäs, F. Zhang and M. R. Andersson, *Chem. Commun.*, 2011, **47**, 4908–4910.

21 E. Wang, Z. Ma, Z. Zhang, K. Vandewal, P. Henriksson, O. Inganäs, F. Zhang and M. R. Andersson, *J. Am. Chem. Soc.*, 2011, **133**, 14244–14247.

22 Z. Ma, E. Wang, M. E. Jarvid, P. Henriksson, O. Inganäs, F. Zhang and M. R. Andersson, *J. Mater. Chem.*, 2012, **22**, 2306–2314.

23 Z. Ma, E. Wang, K. Vandewal, M. R. Andersson and F. Zhang, *Appl. Phys. Lett.*, 2011, **99**, 143302.

24 C. Müller, E. Wang, L. M. Andersson, K. Tvingstedt, Y. Zhou, M. R. Andersson and O. Inganäs, *Adv. Funct. Mater.*, 2010, **20**, 2124–2131.

25 R. C. Coffin, J. Peet, J. Rogers and G. C. Bazan, *Nat. Chem.*, 2009, **1**, 657–661.

26 A. Ajayaghosh, *Chem. Soc. Rev.*, 2003, **32**, 181–191.

27 J.-L. Brédas, D. Beljonne, V. Coropceanu and J. Cornil, *Chem. Rev.*, 2004, **104**, 4971–5004.

28 J.-L. Brédas, J. E. Norton, J. Cornil and V. Coropceanu, *Acc. Chem. Res.*, 2009, **42**, 1691–1699.

29 L. A. A. Pettersson, L. S. Roman and O. Inganäs, *J. Appl. Phys.*, 1999, **86**, 487–496.

368 | *Energy Environ. Sci.*, 2014, **7**, 361–369

This journal is © The Royal Society of Chemistry 2014

30 C. M. Cardona, W. Li, A. E. Kaifer, D. Stockdale and G. C. Bazan, *Adv. Mater.*, 2011, **23**, 2367–2371.

31 V. V. Pavlishchuk and A. W. Addison, *Inorg. Chim. Acta*, 2000, **298**, 97–102.

32 C. Lee, W. Yang and R. G. Parr, *Phys. Rev. B: Condens. Matter Mater. Phys.*, 1988, **37**, 785–789.

33 A. D. Becke, *J. Chem. Phys.*, 1993, **98**, 5648–5652.

34 W. J. Hehre, R. Ditchfield and J. A. Pople, *J. Chem. Phys.*, 1972, **56**, 2257–2261.

35 N. Blouin, A. Michaud, D. Gendron, S. Wakim, E. Blair, R. Neagu-Plesu, M. Belletête, G. Durocher, Y. Tao and M. Leclerc, *J. Am. Chem. Soc.*, 2008, **130**, 732–742.

36 M. C. Scharber, D. Mühlbacher, M. Koppe, P. Denk, C. Waldauf, A. J. Heeger and C. J. Brabec, *Adv. Mater.*, 2006, **18**, 789–794.

37 J. K. Lee, W. L. Ma, C. J. Brabec, J. Yuen, J. S. Moon, J. Y. Kim, K. Lee, G. C. Bazan and A. J. Heeger, *J. Am. Chem. Soc.*, 2008, **130**, 3619–3623.

38 J. T. Rogers, K. Schmidt, M. F. Toney, E. J. Kramer and G. C. Bazan, *Adv. Mater.*, 2011, **23**, 2284–2288.

39 J. C. Bijleveld, A. P. Zoombelt, S. G. J. Mathijssen, M. M. Wienk, M. Turbiez, D. M. de Leeuw and R. A. J. Janssen, *J. Am. Chem. Soc.*, 2009, **131**, 16616–16617.

40 W. Li, K. H. Hendriks, W. S. C. Roelofs, Y. Kim, M. M. Wienk and R. A. J. Janssen, *Adv. Mater.*, 2013, **25**, 3182–3186.

41 M. M. Mandoc, L. J. A. Koster and P. W. M. Blom, *Appl. Phys. Lett.*, 2007, **90**, 133504.

42 W. Tress, K. Leo and M. Riede, *Phys. Rev. B: Condens. Matter Mater. Phys.*, 2012, **85**, 155201.

43 L. Pandey, C. Risko, J. E. Norton and J.-L. Brédas, *Macromolecules*, 2012, **45**, 6405–6414.

44 R. Mondal, S. Ko, J. E. Norton, N. Miyaki, H. A. Becerril, E. Verploegen, M. F. Toney, J.-L. Brédas, M. D. McGehee and Z. Bao, *J. Mater. Chem.*, 2009, **19**, 7195–7197.

45 D. Veldman, O. İpek, S. C. J. Meskers, J. Sweelssen, M. M. Koetse, S. C. Veenstra, J. M. Kroon, S. S. van Bavel, J. Loos and R. A. J. Janssen, *J. Am. Chem. Soc.*, 2008, **130**, 7721–7735.

46 K. Vandewal, K. Tvingstedt, A. Gadisa, O. Inganäs and J. V. Manca, *Nat. Mater.*, 2009, **8**, 904–909.

47 K. Vandewal, A. Gadisa, W. D. Oosterbaan, S. Bertho, F. Banishoeib, I. Van Severen, L. Lutsen, T. J. Cleij, D. Vanderzande and J. V. Manca, *Adv. Funct. Mater.*, 2008, **18**, 2064–2070.

48 K. Vandewal, K. Tvingstedt, A. Gadisa, O. Inganäs and J. V. Manca, *Phys. Rev. B: Condens. Matter Mater. Phys.*, 2010, **81**, 125204.

49 K. Tvingstedt, K. Vandewal, A. Gadisa, F. Zhang, J. Manca and O. Inganäs, *J. Am. Chem. Soc.*, 2009, **131**, 11819–11824.

50 K. Vandewal, L. Goris, I. Haeldermans, M. Nesládek, K. Haenen, P. Wagner and J. V. Manca, *Thin Solid Films*, 2008, **516**, 7135–7138.

51 R. T. Ross, *J. Chem. Phys.*, 1967, **46**, 4590–4593.

52 G. Smestad and H. Ries, *Sol. Energy Mater. Sol. Cells*, 1992, **25**, 51–71.

53 U. Rau, *Phys. Rev. B: Condens. Matter Mater. Phys.*, 2007, **76**, 085303.

54 K. Tvingstedt, K. Vandewal, F. Zhang and O. Inganäs, *J. Phys. Chem. C*, 2010, **114**, 21824–21832.

55 A. C. Morteani, P. Sreearunothai, L. M. Herz, R. H. Friend and C. Silva, *Phys. Rev. Lett.*, 2004, **92**, 247402.

56 L. A. A. Pettersson, L. S. Roman and O. Inganäs, *J. Appl. Phys.*, 2001, **89**, 5564–5569.

57 G. F. Burkhard, E. T. Hoke, S. R. Scully and M. D. McGehee, *Nano Lett.*, 2009, **9**, 4037–4041.

58 P. Scherrer, *Nachrichten von der Gesellschaft der Wissenschaften zu Göttingen*, 1918, **2**, 98–100.

59 S. Lilliu, T. Agostinelli, E. Pires, M. Hampton, J. Nelson and J. E. Macdonald, *Macromolecules*, 2011, **44**, 2725–2734.

60 C. Müller, T. A. M. Ferenczi, M. Campoy-Quiles, J. M. Frost, D. D. C. Bradley, P. Smith, N. Stingelin-Stutzmann and J. Nelson, *Adv. Mater.*, 2008, **20**, 3510–3515.

61 K. D. Sattler, *Handbook of Nanophysics: Clusters and Fullerenes*, CRC Press, 2010.

This journal is © The Royal Society of Chemistry 2014

Energy Environ. Sci., 2014, **7**, 361–369 | **369**